Journal of Computational Applied Mechanics 2026, 57(2): 326-347

DOI: 10.22059/jcamech.2026.410397.1772

RESEARCH PAPER

Langlois' Recursive Approach to Non-Creeping Inertial Viscoelastic Corner Flow in Thin Films

Laraib Mehboob [a], Khadija Maqbool [a], , R. Ellahi [a, b, *], Sadiq M Sait [c, d]

[a] *Department of Mathematics and Statistics, International Islamic University, Islamabad, Pakistan*
[b] *Center for Modeling & Computer Simulation, Research Institute, King Fahd University of Petroleum & Minerals, Dhahran, Saudi Arabia*
[c] *Center for Communications and IT Research, Research Institute, King Fahd University of Petroleum & Minerals, Dhahran-31261, Saudi Arabia*
[d] *Interdisciplinary Research Center for Smart Mobility and Logistics, King Fahd University of Petroleum & Minerals, Dhahran, Saudi Arabia*

Abstract

Dip coating is a key technique in thin film fabrication, widely applied in protective coatings, and material surface engineering. The coating quality depends strongly on the fluid dynamics near substrate edges, where viscoelastic effects and inertial forces can lead to stress concentration and flow instabilities. A viscoelastic fluid model is formulated based on conservation of mass and momentum, with nonlinear governing equations solved using the Langlois recursive approach and the inverse method. Analytical solutions of the stream function provide insight into velocity fields, pressure distribution, and stress behavior near the substrate surface. Results show that stresses and pressure diverge near sharp substrate corners, which can compromise coating durability. Variations in the interface angle significantly alter stress distributions on both the substrate and free surface. Furthermore, inertial forces amplify fluid velocities in the corner region, directly influencing film thickness uniformity and mechanical performance of coated layers.

Keywords: Thin film, Viscoelastic, Inertial forces, Corner flow, Langlois approach.

1. Introduction

Dip coating is a versatile and widely used technique for applying thin films or coatings to a substrate by immersing it into a liquid solution and then withdrawing it at a controlled speed. The process can be defined as depositing aqueous-based liquid-phase coating solutions onto the surface of a substrate. Generally, target materials are dissolved in solutions, which are directly coated on the surface of the substrate. The resulting wet coating is then evaporated to obtain a dry film [1, 2]. The film thickness typically follows the Landau-Levich-Derjaguin (LLD) model [3], which shows that the thickness of the dragged layer is a function of the withdrawal speed. The faster the withdrawal, the thicker

*Corresponding author (R. Ellahi): E-mails: rellahi@alumni.ucr.edu; rahmatellahi@yahoo.com

the coating. This process is widely applied in anti-reflective and protective coatings on lenses and mirrors, coating of semiconductors or insulating layers on devices, and application of sol-gel coatings for thermal or chemical resistance. It is a low-cost, waste-free process that produces uniform coatings over large areas and can easily be scaled up for industrial production.

In dip coating, corner flow occurs near sharp angles or intersections, such as plate-substrate junctions or moving and fixed boundary interfaces. In these regions, geometrical singularities arise where stress or velocity gradients become large. Dip coating processes often involve non-Newtonian fluids that exhibit properties such as shear-thinning or thickening, memory effects, and viscoelasticity. This research focuses on viscoelastic fluids such as polymeric solutions [4] or gel-based fluids carrying drugs or functional particles (for biomedical coatings), conductive fillers (for printed electronics), and ultraviolet-curable or thermal-reactive resins (for protective coatings). The elastic component of viscoelastic fluids slows the thinning of the film during the drainage phase, especially at low withdrawal speeds. This results in thicker coatings than those predicted by Newtonian theory at equivalent speeds.

Researchers have long been intrigued by the study of fluid flow near corners because of its theoretical complexity and practical importance. Goodier [5] was the first to describe the flow created by one of the corner's walls moving steadily parallel to itself. These studies revealed that flow becomes complicated at certain critical corner angles. Moffatt [6] examined the Stokes flow between two crossing planes, rightly indicating that such configurations can generate an infinite series of eddies of decreasing magnitude. Later, Taneda [7] verified these theoretical predictions experimentally by demonstrating the existence of a sequence of diminishing eddies.

In a dihedral corner, Moffatt et al. [8] examined Poiseuille flow. Later, Betelu et al. [9] incorporated additional boundary requirements and discussed viscous flow at a corner, although they ignored surface tension. Although viscous fluids have been studied extensively, the flow of Newtonian fluids over intersecting planes has also been generalized to numerous non-Newtonian fluid models because of their extensive engineering applications. For instance, such studies provide crucial information for the design of industrially significant extrusion dies.

Non-inertial converging flow was explored by Han et al. [10], who considered a modified second-grade fluid model and assumed that each material function depends on the second invariant of the deformation rate. Renardy [11] studied the flow of an upper-convected Maxwell fluid near a corner and concluded that the upstream corner stress is infinite along the entire wall. Siddiqui et al. [12] studied Sisko fluid flow near a corner using a model of Taylor's scraping problem. Spritteles et al. [13] analyzed viscous flows in domains where the boundaries form two-dimensional corners. Chaffin et al. [14] examined Taylor's paint scraping problem, investigating the dynamics of a Carreau fluid and analyzing the flow near and far from the corner. Mahmood [15] examined the effect of inertia on viscous fluid flow near a corner and also observed the effect of leakage at the apex. The interaction of fluid with sharp geometrical changes leads to unique flow structures, such as singularities and vortex formation, which make corner flow a rich area of investigation in fluid mechanics. Because of its importance in both theoretical and applied contexts, corner flow has remained an active area of research. A few core studies on non-creeping, viscoelastic flow, coatings, thin films and most relavant analytical and numerical techniques can be found in [16-25], along with several significant investigations referenced therein.

This study aims to investigate the non-creeping flow of a viscoelastic fluid near a corner using Taylor's scraping problem. It contributes to a deeper understanding of viscoelastic fluid behavior in complex geometries. The laws of conservation of mass and momentum are used to model the problem, and the Langlois recursive technique with the inverse method is employed to solve the resulting nonlinear problem. Velocity and pressure distributions of the fluid are examined near a sharp edge by analyzing their mathematical expressions and graphical results. The normal and tangential stresses on the free surface and the plate are observed at the corner and at different interface angles. This research also provides a comparison between Stokes and inertial flow of viscoelastic fluid near a corner using graphical results.

2. Formulation of the problem

Consider a dip coating problem in which a plate is pulled out of a stationary liquid bath (i.e., a viscoelastic fluid) at a steady speed $\boldsymbol{V} = (-\varepsilon U, 0)$. The liquid wets the plate, and a corner flow is formed between the plate and the free surface interface (meniscus), making an angle $\theta = \theta_0$ (i.e., the interface angle), as shown in Figure 1. For the mathematical analysis, a polar coordinate system (r, θ) is adopted, with the origin placed at the point of intersection of the plate and the meniscus.

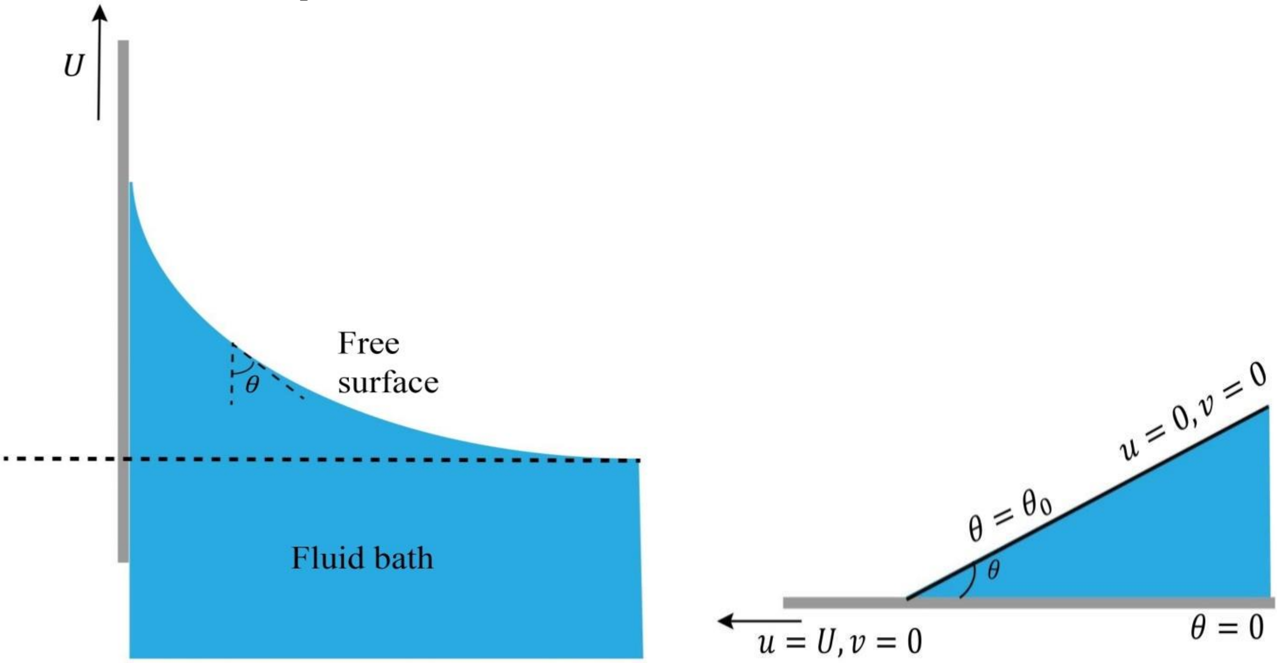

(a) **(b)**

Figure 1: Geometry of the problem

The following velocity field is assumed for dip coating:

$$\boldsymbol{V} = (u(r,\theta), v(r,\theta)), \tag{1}$$

The free surface and the moving plate which is immersed in fluid suggest the following boundary conditions:

$$u(r,\theta) = -\varepsilon U, \quad v(r,\theta) = 0 \quad at \quad \theta = 0, \tag{2}$$

$$u(r,\theta) = 0, \quad v(r,\theta) = 0 \quad at \quad \theta = \theta_0. \tag{3}$$

The viscoelastic flow properties through a corner can be studied by the following continuity and momentum equations:

$$\nabla.\boldsymbol{V} = 0, \tag{4}$$

$$\frac{\rho D\boldsymbol{V}}{Dt} = -\nabla p + div\boldsymbol{S}, \tag{5}$$

where ρ stands for fluid density which is constant in the flow field, p is the dynamic pressure and $\boldsymbol{S}$ is extra stress tensor of viscoelastic fluid.

After using Eq. (1) into Eqs. (4) and (5), one can get the following form:

$$\frac{1}{r}\frac{\partial(ru)}{\partial r} + \frac{1}{r}\frac{\partial v}{\partial \theta} = 0, \tag{6}$$

r-component of momentum equation

$$\rho\left(u\frac{\partial u}{\partial r} + \frac{v}{r}\frac{\partial u}{\partial \theta} - \frac{v^2}{r}\right) = -\frac{\partial p}{\partial r} + \frac{1}{r}\frac{\partial}{\partial r}(rS_{rr}) + \frac{1}{r}\frac{\partial S_{r\theta}}{\partial \theta} - \frac{S_{\theta\theta}}{r}, \tag{7}$$

θ-component of momentum equation

$$\rho\left(u\frac{\partial v}{\partial r} + \frac{v}{r}\frac{\partial v}{\partial \theta} + \frac{uv}{r}\right) = -\frac{1}{r}\frac{\partial p}{\partial \theta} + \frac{1}{r^2}\frac{\partial(r^2 S_{r\theta})}{\partial r} + \frac{1}{r}\frac{\partial S_{\theta\theta}}{\partial \theta}, \tag{8}$$

Where S_{rr}, $S_{\theta\theta}$ and $S_{r\theta}$ are normal and tangential components of stress tensor.

The extra stress tensor $\boldsymbol{S}$ of viscoelastic fluid satisfies the following relation:

$$\left(1 + \lambda\frac{D}{Dt}\right)\boldsymbol{S} = \mu\boldsymbol{A_1}, \tag{9}$$

where

$$\frac{D\boldsymbol{S}}{Dt} = (\boldsymbol{V}.\nabla)\boldsymbol{S} - (\nabla\boldsymbol{V})\boldsymbol{S} - \boldsymbol{S}(\nabla\boldsymbol{V})^T, \tag{10}$$

$$\boldsymbol{A_1} = \nabla\boldsymbol{V} + (\nabla\boldsymbol{V})^T, \tag{11}$$

In above expression $\frac{D}{Dt}$ is the material derivative, $\boldsymbol{A_1}$ is the first Rivlin-Ericksen tensor, λ and μ represent the relaxation time and the dynamic viscosity respectively.

3. Solution of the problem

To solve the Eqs. (6)-(8) we will adopt the Langlois Recursive technique [26, 27] introduced by William E. Langlois, which manages nonlinearity of the system and provides a hierarchy of linear or simpler equations to solve recursively. In this technique the velocity profile, pressure and shear stress become linear with the help of a small dimensionless number ε.

It is assumed that series solution for velocity, shear stress and pressure is given in the following form:

$$\boldsymbol{V}(r,\theta) = \sum_{k=1}^{\infty} \varepsilon^k \boldsymbol{V}^{(k)}(r,\theta), \tag{12}$$

$$\boldsymbol{S}(r,\theta) = \sum_{k=1}^{\infty} \varepsilon^k \boldsymbol{S}^{(k)}(r,\theta), \tag{13}$$

$$p(r,\theta) = constant + \sum_{k=1}^{\infty} \varepsilon^k p^{(k)}(r,\theta), \tag{14}$$

The velocity and pressure considered for this problem is given in the following form:

$$\boldsymbol{V}^{(k)} = \left(u^{(k)}(r,\theta), v^{(k)}(r,\theta)\right), \tag{15}$$

$$p^{(k)} = p^{(k)}(r,\theta), \tag{16}$$

Associated boundary conditions are

$$\boldsymbol{V}^{(1)} = (-\varepsilon U, 0), \;\; at \;\; \theta = 0, \tag{17}$$

$$\boldsymbol{V}^{(k)} = (0,0), k > 1 \;\; at \;\; \theta = 0, \tag{18}$$

$$\boldsymbol{V}^{(k)} = (0,0), k \geq 1 \;\; at \;\; \theta = \theta_0. \tag{19}$$

To get dimensionless form of Eqs. (6)-(11), following dimensionless quantities are considered:

$$u^{(k)'} = \frac{u^{(k)}}{U_0}, v^{(k)'} = \frac{v^{(k)}}{U_0}, U^{(k)'} = \frac{U^{(k)}}{U_0}, r' = \frac{r}{R}, p^{(k)'} = \frac{p^{(k)}}{\mu U_0/_R},$$

$$Wi = \frac{\lambda U_0}{R}, \boldsymbol{S}^{(k)'} = \frac{\boldsymbol{S}^{(k)}}{\mu U_0/_R}, Re = \frac{\rho U_0 R}{\mu}. \tag{20}$$

For analytical tractability, we limit our analysis up to third order in ε, neglecting all higher-order contributions due to the increasing complexity of the resulting equations. Using Eqs. (12)-(19) in Eqs. (6)-(11), and collecting the terms of $\varepsilon, \varepsilon^2$ and ε^3 one can get the first, second and third-order systems and their solutions.

3.1: First-order problem and its solution

The dimensionless form of first order problem is represented as follows:

$$\frac{\partial u^{(1)}}{\partial r} + \frac{1}{r}\frac{\partial v^{(1)}}{\partial \theta} + \frac{u^{(1)}}{r} = 0, \tag{21}$$

$$\frac{\partial p^{(1)}}{\partial r} = \frac{1}{r}\frac{\partial}{\partial r}\left(rS_{rr}^{(1)}\right) + \frac{1}{r}\frac{\partial S_{r\theta}^{(1)}}{\partial \theta} - \frac{S_{\theta\theta}^{(1)}}{r}, \tag{22}$$

$$\frac{1}{r}\frac{\partial p^{(1)}}{\partial \theta} = \frac{1}{r^2}\frac{\partial\left(r^2 S_{r\theta}^{(1)}\right)}{\partial r} + \frac{1}{r}\frac{\partial S_{\theta\theta}^{(1)}}{\partial \theta}, \tag{23}$$

where components of stress tensor in dimensionless form are mentioned as below:

$$S_{rr}^{(1)} = 2\frac{\partial u^{(1)}}{\partial r}, \;\; S_{r\theta}^{(1)} = S_{\theta r}^{(1)} = \frac{\partial v^{(1)}}{\partial r} + \frac{1}{r}\frac{\partial u^{(1)}}{\partial \theta} - \frac{v^{(1)}}{r}, \;\; S_{\theta\theta}^{(1)} = \frac{2}{r}\left(\frac{\partial v^{(1)}}{\partial \theta} + u^{(1)}\right). \tag{24}$$

Using Eq. (24), the continuity and momentum equation of first order reduces into the following form

$$\frac{\partial u^{(1)}}{\partial r} + \frac{1}{r}\frac{\partial v^{(1)}}{\partial \theta} + \frac{u^{(1)}}{r} = 0, \tag{25}$$

$$\frac{\partial p^{(1)}}{\partial r} = \nabla^2 u^{(1)} + \frac{2}{r}\frac{\partial u^{(1)}}{\partial r} + \frac{u^{(1)}}{r^2}, \tag{26}$$

$$\frac{\partial p^{(1)}}{\partial \theta} = \nabla^2 v^{(1)} + \frac{2}{r^2}\frac{\partial u^{(1)}}{\partial \theta} - \frac{v^{(1)}}{r^2}, \tag{27}$$

where

$$\nabla^2 = \frac{\partial^2}{\partial r^2} + \frac{1}{r^2}\frac{\partial^2}{\partial \theta^2} + \frac{1}{r}\frac{\partial}{\partial r}, \tag{28}$$

The boundary conditions are mentioned as below:

$$u^{(1)} = -U, v^{(1)} = 0, \quad at \ \ \theta = 0, \tag{29}$$

$$u^{(1)} = 0, v^{(1)} = 0, \quad at \ \ \theta = \theta_0. \tag{30}$$

To reduce the number of unknown and equations we will introduce the following stream function $\Psi^{(1)}(r,\theta)$:

$$u^{(1)} = \frac{1}{r}\frac{\partial \Psi^{(1)}}{\partial \theta}, \quad v^{(1)} = -\frac{\partial \Psi^{(1)}}{\partial r}. \tag{31}$$

Cross-differentiating Eq. (26) and (27) eliminates pressure and then substituting Eq. (31) in the resulting equation one can get the following expressions:

$$\nabla^4 \Psi^{(1)} = 0, \tag{32}$$

with the following boundary conditions

$$\frac{\partial \Psi^{(1)}}{\partial \theta} = -Ur, \qquad \Psi^{(1)} = 0, \quad at \ \ \theta = 0, \tag{33}$$

$$\frac{\partial \Psi^{(1)}}{\partial \theta} = 0 = \Psi^{(1)}, \qquad at \ \ \theta = \theta_0. \tag{34}$$

Assuming the solution of first-order stream function [28] in the following form

$$\Psi^{(1)} = Urf(\theta). \tag{35}$$

After using Eq. (35) in Eqs. (32)-(34) and then solving the resulting differential equation, the velocity components of first order $u^{(1)}$ and $v^{(1)}$ are expressed as

$$u^{(1)} = Uf'(\theta), \qquad v^{(1)} = -Uf(\theta). \tag{36}$$

For a pressure of first order, we use Eq. (36) in Eqs. (26) & (27)

$$\frac{\partial p^{(1)}}{\partial r} = \frac{U}{r^2} g'(\theta), \tag{37}$$

$$\frac{\partial p^{(1)}}{\partial \theta} = \frac{U}{r} g(\theta), \tag{38}$$

In which $g(\theta) = f(\theta) + f''(\theta)$.

Integrating Eq. (37) with respect to r and then differentiating the resulting expression with respect to θ, after comparing the expression with Eq. (38), we get the pressure for first order:

$$p^{(1)} = -\frac{U}{r} g'(\theta) + p_0, \tag{39}$$

Where p_0 is constant and it shows the singularity near $r = 0$.

3.2: Second-order problem and its solution

Dimensionless form of continuity and momentum equation for second order is given in the following form:

$$\frac{\partial u^{(2)}}{\partial r} + \frac{1}{r}\frac{\partial v^{(2)}}{\partial \theta} + \frac{u^{(2)}}{r} = 0, \tag{40}$$

$$Re\left(u^{(1)}\frac{\partial u^{(1)}}{\partial r} + \frac{v^{(1)}}{r}\frac{\partial u^{(1)}}{\partial \theta} - \frac{{v^{(1)}}^2}{r}\right) = -\frac{\partial p^{(2)}}{\partial r} + \frac{1}{r}\frac{\partial}{\partial r}\left(rS_{rr}^{(2)}\right) + \frac{1}{r}\frac{\partial S_{r\theta}^{(2)}}{\partial \theta} - \frac{S_{\theta\theta}^{(2)}}{r}, \tag{41}$$

$$Re\left(u^{(1)}\frac{\partial v^{(1)}}{\partial r}+\frac{v^{(1)}}{r}\frac{\partial v^{(1)}}{\partial \theta}+\frac{u^{(1)}v^{(1)}}{r}\right)=-\frac{1}{r}\frac{\partial p^{(2)}}{\partial \theta}+\frac{1}{r^2}\frac{\partial\left(r^2 S_{r\theta}^{(2)}\right)}{\partial r}+\frac{1}{r}\frac{\partial S_{\theta\theta}^{(2)}}{\partial \theta}, \tag{42}$$

Where dimensionless stress tensor components of the second order are mentioned as follows:

$$S_{rr}^{(2)}=2\frac{\partial u^{(2)}}{\partial r},\quad S_{r\theta}^{(2)}=S_{\theta r}^{(2)}=\frac{WiU^2}{r^2}(fg)'+\frac{\partial v^{(2)}}{\partial r}+\frac{1}{r}\frac{\partial u^{(2)}}{\partial \theta}-\frac{v^{(2)}}{r}, \tag{43}$$

$$S_{\theta\theta}^{(2)}=\frac{2WiU^2g^2}{r^2}+\frac{2}{r}\left(\frac{\partial v^{(2)}}{\partial \theta}+u^{(2)}\right), \tag{44}$$

After using Eqs. (43) and (44) in Eqs. (41) and (42), the above momentum equation takes the following form:

$$\frac{\partial p^{(2)}}{\partial r}=\frac{U^2Re}{r}(ff''+f^2)+\frac{WiU^2}{r^3}((fg)''-2g^2)+\nabla^2u^{(2)}+\frac{2}{r}\frac{\partial u^{(2)}}{\partial r}+\frac{u^{(2)}}{r^2}, \tag{45}$$

$$\frac{\partial p^{(2)}}{\partial \theta}=\frac{4WiU^2}{r^2}gg'+\nabla^2v^{(2)}+\frac{2}{r^2}\frac{\partial u^{(2)}}{\partial \theta}-\frac{v^{(2)}}{r^2}, \tag{46}$$

And boundary conditions are mentioned below:

$$u^{(2)}=0, v^{(2)}=0,\quad at\ \theta=0, \tag{47}$$

$$u^{(2)}=0, v^{(2)}=0,\quad at\ \theta=\theta_0. \tag{48}$$

The following stream functions reduce the problem in simple and compact form:

$$u^{(2)}=\frac{1}{r}\frac{\partial \Psi^{(2)}}{\partial \theta},\quad v^{(2)}=-\frac{\partial \Psi^{(2)}}{\partial r}, \tag{49}$$

By using the same procedure as done in first order one can get the following form:

$$\nabla^4\Psi^{(2)}=-\frac{U^2Re}{r^2}((ff'')'+2ff')-\frac{WiU^2}{r^4}[(fg)'''+4gg'], \tag{50}$$

The corresponding boundary conditions take the following form:

$$\frac{\partial \Psi^{(2)}}{\partial \theta}=0,\qquad \Psi^{(2)}=0,\quad at\ \theta=0, \tag{51}$$

$$\frac{\partial \Psi^{(2)}}{\partial \theta}=0=\Psi^{(2)},\qquad at\ \theta=\theta_0. \tag{52}$$

Let

$$\Psi^{(2)}=WiU^2f_1(\theta)+ReU^2r^2f_2(\theta), \tag{53}$$

be the assumed solution. After using the above assumption given in Eqs. (50)-(52), one can get the following expression:

$$\frac{WiU^2}{r^4}\left(f_1^{(iv)}+4f_1''\right)+\frac{U^2Re}{r^2}\left(f_2^{(iv)}+4f_2''\right)=-\frac{U^2Re}{r^2}((ff'')'+2ff')-\frac{WiU^2}{r^4}[(fg)'''+4gg'], \tag{54}$$

After comparison on both sides one can get the following systems of equations:

$$f_1^{(iv)}+4f_1''=-[(fg)'''+4gg'], \tag{55}$$

$$f_1'(\theta)=0, f_1(\theta)=0\ \ when\ \theta=0, \tag{56}$$

$$f_1'(\theta)=0, f_1(\theta)=0\ when\ \theta=\theta_0. \tag{57}$$

$$f_2^{(iv)}+4f_2''=-((ff'')'+2ff'), \tag{58}$$

$$f_2(\theta)=0, f_2'(\theta)=0\ \ when\ \theta=0, \tag{59}$$

$$f_2(\theta)=0, f_2'(\theta)=0\ when\ \theta=\theta_0. \tag{60}$$

The solution of above BVPs are calculated by software Mathematica 12.0.

After getting the solutions, one can find the explicit expression of stream function of second order that will help to find following second-order velocity components:

$$u^{(2)} = U^2\left(\frac{Wi}{r}f_1'(\theta) + Re\, rf_2'(\theta)\right),\ \ v^{(2)} = -2ReU^2rf_2(\theta). \tag{61}$$

After using $u^{(2)}$ and $v^{(2)}$ from Eq. (61) in Eqs. (45) and (46) and then integrating (45) with respect to r and then taking the partial derivative of the resulting expression with respect to θ and then comparing with Eq. (46) one can get the following expression of second-order pressure:

$$p^{(2)} = \frac{2WiU^2}{r^2}(f_1' + g^2) + p_2, \tag{62}$$

Where p_2 is constant and it involves the singularity of second order.

3.3: Third-order problem and its solution

For the third-order problem the dimensionless form of continuity and momentum takes the following form

$$\frac{\partial u^{(3)}}{\partial r} + \frac{1}{r}\frac{\partial v^{(3)}}{\partial \theta} + \frac{u^{(3)}}{r} = 0, \tag{63}$$

$$Re\left(u^{(1)}\frac{\partial u^{(2)}}{\partial r} + u^{(2)}\frac{\partial u^{(1)}}{\partial r} + \frac{v^{(1)}}{r}\frac{\partial u^{(2)}}{\partial \theta} + \frac{v^{(2)}}{r}\frac{\partial u^{(1)}}{\partial \theta} - \frac{2v^{(1)}v^{(2)}}{r}\right)$$
$$= -\frac{\partial p^{(3)}}{\partial r} + \frac{1}{r}\frac{\partial}{\partial r}\left(rS_{rr}^{(3)}\right) + \frac{1}{r}\frac{\partial S_{r\theta}^{(3)}}{\partial \theta} - \frac{S_{\theta\theta}^{(3)}}{r}, \tag{64}$$

$$Re\left(u^{(1)}\frac{\partial v^{(2)}}{\partial r} + u^{(2)}\frac{\partial v^{(1)}}{\partial r} + \frac{v^{(1)}}{r}\frac{\partial v^{(2)}}{\partial \theta} + \frac{v^{(2)}}{r}\frac{\partial v^{(1)}}{\partial \theta} + \frac{u^{(1)}v^{(2)}}{r} + \frac{u^{(2)}v^{(1)}}{r}\right)$$
$$= -\frac{1}{r}\frac{\partial p^{(3)}}{\partial \theta} + \frac{1}{r^2}\frac{\partial\left(r^2S_{r\theta}^{(3)}\right)}{\partial r} + \frac{1}{r}\frac{\partial S_{\theta\theta}^{(3)}}{\partial \theta}, \tag{65}$$

Where third-order components of stress tensor are expressed as follows:

$$S_{rr}^{(3)} = 2\frac{\partial u^{(3)}}{\partial r} - \frac{2WiU^3}{r}\left(\frac{Wi}{r^2}b_1(\theta) + Reb_2(\theta)\right), \tag{66}$$

$$S_{r\theta}^{(3)} = S_{\theta r}^{(3)} = -\frac{2WiU^3}{r}\left(\frac{Wi}{r^2}b_3(\theta) + Reb_4(\theta)\right) + \frac{\partial v^{(3)}}{\partial r} + \frac{1}{r}\frac{\partial u^{(3)}}{\partial \theta} - \frac{v^{(3)}}{r}, \tag{67}$$

$$S_{\theta\theta}^{(3)} = -\frac{2WiU^3}{r}\left(\frac{Wi}{r^2}b_5(\theta) + Reb_6(\theta)\right) + \frac{2}{r}\left(\frac{\partial v^{(3)}}{\partial \theta} + u^{(3)}\right), \tag{68}$$

Where $b_i, i = 1,2,\dots,6$ are defined in appendix.

After using Eqs. (66)-(68) in Eqs. (64) and (65) the dimensionless form of the momentum equation takes the following form:

$$\frac{\partial p^{(3)}}{\partial r} = \nabla^2 u^{(3)} + \frac{2}{r}\frac{\partial u^{(3)}}{\partial r} + \frac{u^{(3)}}{r^2} + U^3\left(\frac{WiRed_1(\theta)}{r^2} + Re^2d_2(\theta) + \frac{Wi^2d_3(\theta)}{r^4}\right), \tag{69}$$

$$\frac{\partial p^{(3)}}{\partial \theta} = \nabla^2 v^{(3)} + \frac{2}{r^2}\frac{\partial u^{(3)}}{\partial \theta} - \frac{v^{(3)}}{r^2} + U^3\left(\frac{WiRed_5(\theta)}{r} + Re^2rd_4(\theta) + \frac{Wi^2d_6(\theta)}{r^3}\right), \tag{70}$$

Along with the following boundary conditions:

$$u^{(3)} = 0, v^{(3)} = 0,\ \ at\ \theta = 0, \tag{71}$$
$$u^{(3)} = 0, v^{(3)} = 0,\ \ at\ \theta = \theta_0. \tag{72}$$

After introducing the following stream function above system of equations reduces into single partial differential equation in one variable:

$$u^{(3)} = \frac{1}{r}\frac{\partial \Psi^{(3)}}{\partial \theta}, \quad v^{(3)} = -\frac{\partial \Psi^{(3)}}{\partial r}, \tag{73}$$

$$\nabla^4 \Psi^{(3)} = U^3\left(-\frac{WiRe}{r^3}(d_1' + d_5) + \frac{Re^2}{r}(-d_2' + d_4) - \frac{Wi^2}{r^5}(d_3' + 3d_6)\right), \tag{74}$$

And boundary conditions take the following form:

$$\frac{\partial \Psi^{(3)}}{\partial \theta} = 0, \quad \Psi^{(3)} = 0, \ at \ \theta = 0, \tag{75}$$

$$\frac{\partial \Psi^{(3)}}{\partial \theta} = 0 = \Psi^{(3)}, \quad at \ \theta = \theta_0. \tag{76}$$

The following assumed solution will help to reduce the above problem into system of linear ODEs

$$\Psi^{(3)} = ReWiU^3 r g_1(\theta) + Re^2U^3r^3 g_2(\theta) + \frac{Wi^2U^3}{r} g_3(\theta), \tag{77}$$

After using Eq. (77) in Eqs. (74)-(76), one can get the following form:

$$\frac{ReWi}{r^2}\left(g_1^{(iv)} + 2g_1'' + g_1\right) + Re^2\left(g_2^{(iv)} + 10g_2'' + 9g_2\right) + \frac{Wi^2}{r^4}\left(g_3^{(iv)} + 10g_3'' + 9g_3\right)$$
$$= -\frac{ReWi}{r^2}(d_1' + d_5) + Re^2(-d_2' + d_4) - \frac{Wi^2}{r^4}(d_3' + 3d_6), \tag{78}$$

After comparing like terms, one can get the following system of ordinary differential equations

$$g_1^{(iv)} + 2g_1'' + g_1 = -(d_1' + d_5), \tag{79}$$
$$g_1'(\theta) = 0, g_1(\theta) = 0 \ \ when\ \theta = 0, \tag{80}$$
$$g_1'(\theta) = 0, g_1(\theta) = 0 \ when\ \theta = \theta_0. \tag{81}$$
$$g_2^{(iv)} + 10g_2'' + 9g_2 = -d_2' + d_4, \tag{82}$$
$$g_2(\theta) = 0, g_2'(\theta) = 0 \ \ when\ \theta = 0, \tag{83}$$
$$g_2(\theta) = 0, g_2'(\theta) = 0 \ when\ \theta = \theta_0. \tag{84}$$
$$g_3^{(iv)} + 10g_3'' + 9g_3 = -(d_3' + 3d_6), \tag{85}$$
$$g_3(\theta) = 0, g_3'(\theta) = 0 \ \ when\ \theta = 0, \tag{86}$$
$$g_3(\theta) = 0, g_3'(\theta) = 0 \ when\ \theta = \theta_0. \tag{87}$$

The solutions of Eqs. (79)-(87) are calculated by software Mathematica 12.0.

After finding the above solutions, one can find the third-order stream function that will used to find the following velocity components:

$$u^{(3)} = U^3\left(ReWig_1'(\theta) + Re^2r^2g_2'(\theta) + \frac{Wi^2}{r^2}g_3'(\theta)\right), \tag{88}$$

$$v^{(3)} = U^3\left(-ReWig_1(\theta) - 3Re^2r^2g_2(\theta) + \frac{Wi^2}{r^2}g_3(\theta)\right). \tag{89}$$

After using $u^{(3)}$ and $v^{(3)}$ from Eqs. (88) and (89) in Eqs. (69) and (70) and then integrating (69) with respect to r and then taking the partial derivative of the resulting expression with respect to θ and comparing with Eq. (70) we get the expression of pressure:

$$p^{(3)} = U^3\left[Re^2 r(-g_2' + d_7) + \frac{ReWi}{r}(g_1' + d_8) + \frac{Wi^2}{r^3}(3g_3' + d_9)\right] + p_3, \tag{90}$$

Where p_3 is constant and $d_i, i = 1,2,\dots,9$ are define in appendix.

Note that in a first-order problem, the singularity occurs at a sharp bend (i.e., $r = 0$) only in the pressure field but velocity is finite everywhere while the second-order and third-order problem solutions give singularity in both fields which conveys the complex flow at a corner.

Summarizing results up to the third order:

$$u(r,\theta) = u^{(1)}(r,\theta) + u^{(2)}(r,\theta) + u^{(3)}(r,\theta), \tag{91}$$

$$v(r,\theta) = v^{(1)}(r,\theta) + v^{(2)}(r,\theta) + v^{(3)}(r,\theta), \tag{92}$$

$$p(r,\theta) = p^{(1)}(r,\theta) + p^{(2)}(r,\theta) + p^{(3)}(r,\theta), \tag{93}$$

$$S_{rr} = S_{rr}{}^{(1)} + S_{rr}{}^{(2)} + S_{rr}{}^{(3)}, \tag{94}$$

$$S_{r\theta} = S_{r\theta}{}^{(1)} + S_{r\theta}{}^{(2)} + S_{r\theta}{}^{(3)}, \tag{95}$$

$$S_{\theta\theta} = S_{\theta\theta}{}^{(1)} + S_{\theta\theta}{}^{(2)} + S_{\theta\theta}{}^{(3)}. \tag{96}$$

The tangential and normal stress is

$$T_t = S_{r\theta}|_{\theta=\theta_0}, T_n = S_{\theta\theta}|_{\theta=\theta_0}, \tag{97}$$

Using Eqs. (95) and (96) in Eq. (97) one can get the following expression of tangential and normal stress:

$$T_n = \frac{32U^3 Wi(\theta_0 \text{Cos}\theta_0 - \text{Sin}\theta_0)^2}{r^2(-1 + 2\theta_0^2 + \text{Cos}\theta_0)^2}, \tag{98}$$

$$T_t = \frac{U^2 \text{Csc}^2\theta_0 \text{Sec}\theta_0 (r^2 ReUa_1 + 4UWia_2 + 128\theta_0 ra_3 + 64ra_4)}{128r^2(-1 + 2\theta_0^2 + \text{Cos}2\theta_0)^2(\theta_0 \text{Csc}\theta_0 - \text{Sec}\theta_0)}. \tag{99}$$

It can be observed from Eqs. (98) and (99) that normal and tangential stresses to the free surface are infinite at $r = 0$.

Taylor [29] said, "In any real situation continuous contact between the free surface and plate will not occur so that infinite stress at $r = 0$ will be relieved over a region comparable with the width of the gap."

Then the component L of the total stress perpendicular to the plate and the component D parallel to the plate are defined as follows:

$$L = T_n cos\theta_0 + T_t sin\theta_0, \tag{100}$$

$$D = T_n sin\theta_0 - T_t cos\theta_0. \tag{101}$$

4. Validation of results

To check the validation of the results obtained from Recursive approach we will find the residues by substituting the solution given in equations (91)-(96) into Eqs. (7) and (8). The error $E_1(r,\theta)$ and $E_2(r,\theta)$ are shown in Tables 1 and 2 which show that momentum equations having small error and demonstrate the accuracy and reliability of the results obtained in this study.

$$E_1(r,\theta) = \rho\left(u^{(1)}\frac{\partial u^{(1)}}{\partial r} + \frac{v^{(1)}}{r}\frac{\partial u^{(1)}}{\partial \theta} - \frac{{v^{(1)}}^2}{r} + u^{(1)}\frac{\partial u^{(2)}}{\partial r} + u^{(2)}\frac{\partial u^{(1)}}{\partial r} + \frac{v^{(1)}}{r}\frac{\partial u^{(2)}}{\partial \theta} + \frac{v^{(2)}}{r}\frac{\partial u^{(1)}}{\partial \theta} - \frac{2v^{(1)}v^{(2)}}{r}\right) + \frac{\partial\left(p^{(1)} + p^{(2)} + p^{(3)}\right)}{\partial r} - \frac{1}{r}\frac{\partial}{\partial r}\left[r\left(S_{rr}^{(1)} + S_{rr}^{(2)} + S_{rr}^{(3)}\right)\right]$$

$$-\frac{1}{r}\frac{\partial\left(S_{r\theta}^{(1)}+S_{r\theta}^{(2)}+S_{r\theta}^{(3)}\right)}{\partial\theta}+\frac{\left(S_{\theta\theta}^{(1)}+S_{\theta\theta}^{(2)}+S_{\theta\theta}^{(3)}\right)}{r}, \tag{102}$$

$$E_2(r,\theta)=\rho\left(u^{(1)}\frac{\partial v^{(1)}}{\partial r}+\frac{v^{(1)}}{r}\frac{\partial v^{(1)}}{\partial\theta}+\frac{u^{(1)}v^{(1)}}{r}+u^{(1)}\frac{\partial v^{(2)}}{\partial r}+u^{(2)}\frac{\partial v^{(1)}}{\partial r}+\frac{v^{(1)}}{r}\frac{\partial v^{(2)}}{\partial\theta}+\frac{v^{(2)}}{r}\frac{\partial v^{(1)}}{\partial\theta}\right.$$
$$\left.+\frac{u^{(1)}v^{(2)}}{r}+\frac{u^{(2)}v^{(1)}}{r}\right)+\frac{1}{r}\frac{\partial\left(p^{(1)}+p^{(2)}+p^{(3)}\right)}{\partial\theta}-\frac{1}{r^2}\frac{\partial\left[r^2\left(S_{r\theta}^{(1)}+S_{r\theta}^{(2)}+S_{r\theta}^{(3)}\right)\right]}{\partial r}$$

$$-\frac{1}{r}\frac{\partial\left(S_{\theta\theta}^{(1)}+S_{\theta\theta}^{(2)}+S_{\theta\theta}^{(3)}\right)}{\partial\theta}. \tag{103}$$

4.1. Special cases

The following results can be deduced from this study

- When $Re\rightarrow 0$ and $Wi=0$ then the radial and azimuthal velocity of the second and third order become zero and the results are reduced for creeping flow of Newtonian fluid [31].
- When $Re\rightarrow 0$ and $Wi\neq 0$, then results for the creeping flow of Maxwell fluid can be obtained [33].
- And when $Re\neq 0$ and $Wi=0$, then results are reduced for the non-creeping flow of Newtonian fluid [33].

5. Results and discussion

This section is organized into four subsections, each focusing on the impact of key physical parameters.

5.1. Velocity field

The results presented in Figures 2 and 3 describe how different parameters affect the velocity distribution of the fluid, particularly near the corner region where the plate emerges from the bath. Figures 2a and 3a show that the fluid velocity increases as the plate length r increases. This occurs because a longer moving plate remains in contact with the fluid over a greater distance, imparting more cumulative shear stress along its surface. The continuous pulling effect accelerates more fluid upward, and the influence is especially pronounced near the corner, where the fluid transitions from the bath to the free surface. Figures 2b and 3b illustrate the effect of plate speed on velocity. A higher plate speed transfers greater momentum to the fluid through enhanced shear stress at the interface. Near the corner, this shear becomes particularly intense due to flow redirection, resulting in a significant rise in fluid velocity. The influence of the Reynolds number, as shown in Figures 2c and 3c, indicates that higher Re values correspond to stronger inertial effects compared to viscous resistance. This inertial dominance promotes greater fluid motion near the corner. Figure 2d examines the effect of the Weissenberg number on viscoelastic fluid velocity. When the Weissenberg number is less than unity, elastic effects are weak, and the fluid behaves more like a purely viscous fluid, especially near the corner region where deformation is highest. Finally, Figure 4 compares inertial and non-inertial cases, showing that velocity near the corner is higher in the presence of inertial forces, as inertia helps sustain motion beyond what viscous forces alone can generate. Overall, these observations demonstrate that geometric effects, plate motion, fluid elasticity, and inertial forces act together to control velocity profiles in the corner region.

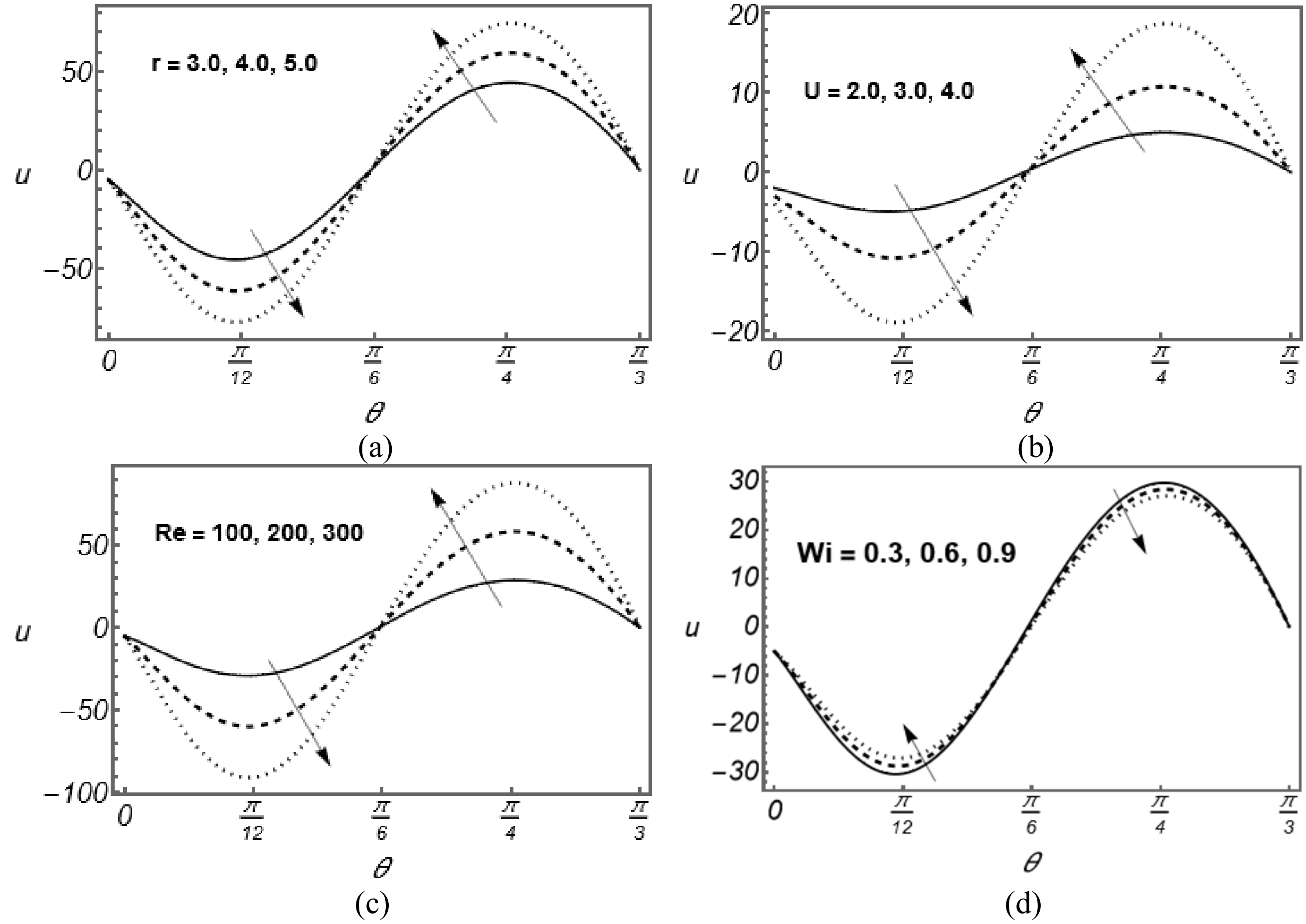

Figure 2: Variation in radial velocity $u(r,\theta)$ for r, U, Re and Wi.

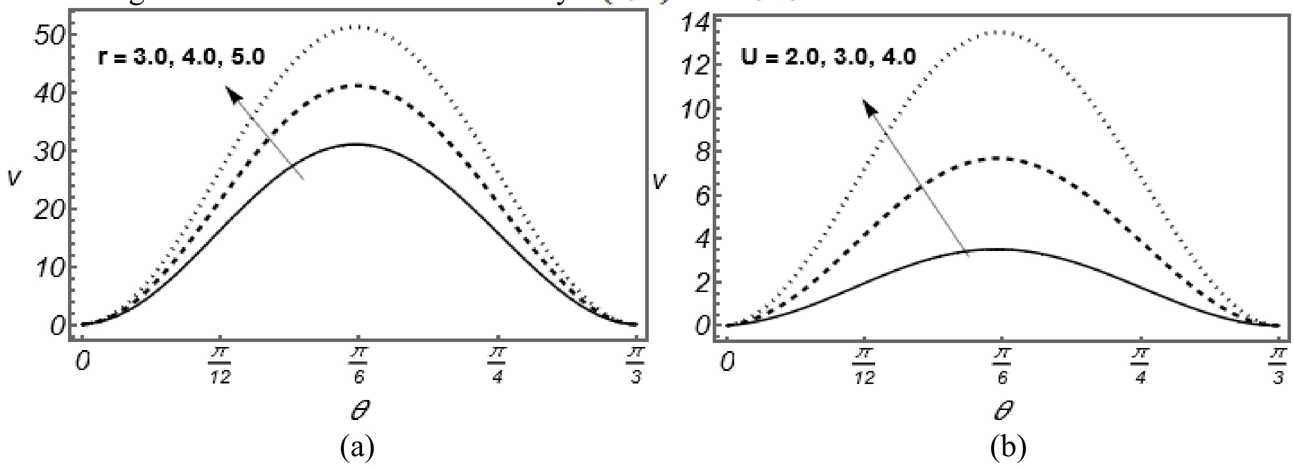

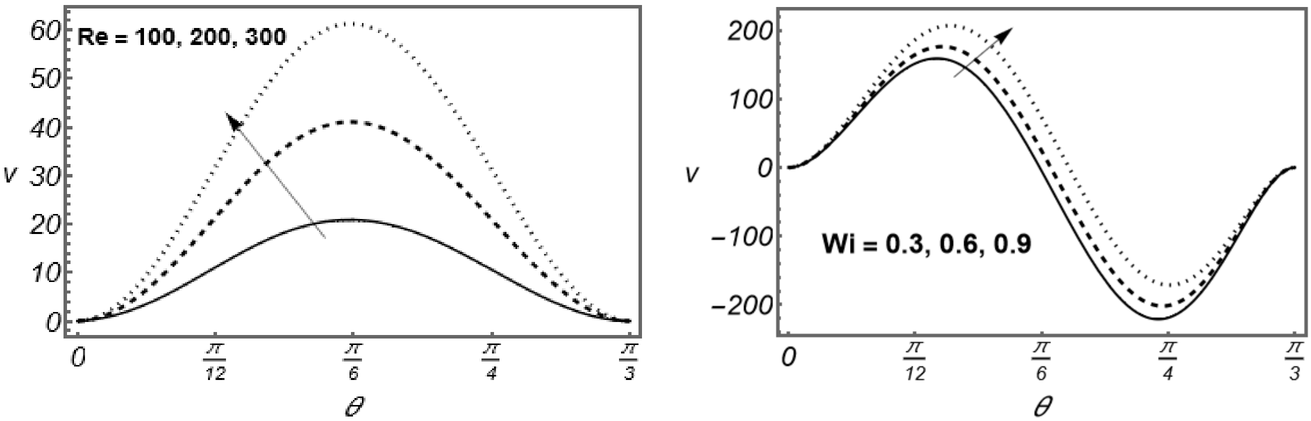

(c) (d)

Figure 3: Variation in azimuthal velocity $v(r,\theta)$ for r, U, Re and Wi.

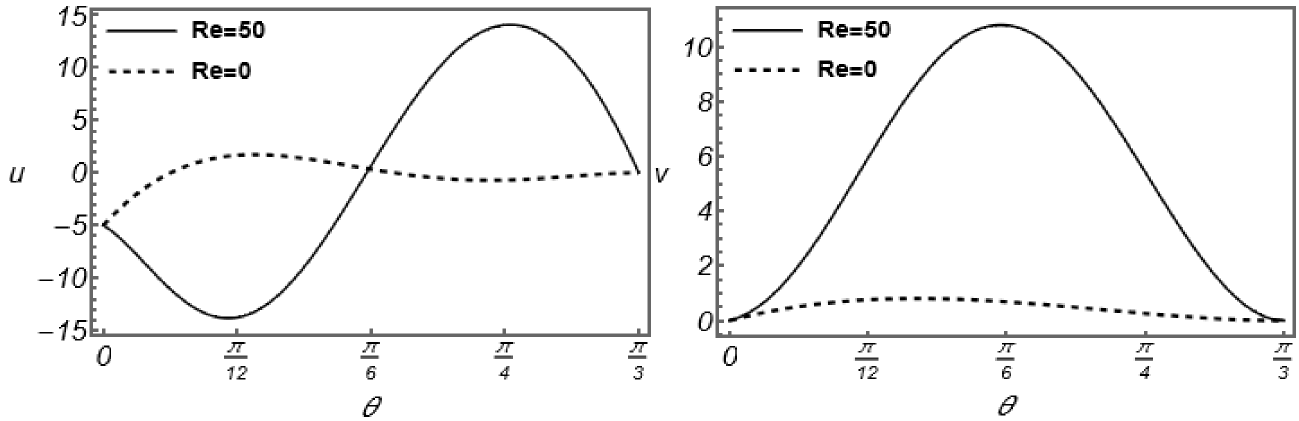

(a) (b)

Figure 4: Comparison between radial and azimuthal velocity for inertial and non-inertial flow.

5.2. Normal and tangential stresses

The graphical results presented in Figures 5 and 6 illustrate how normal and tangential stresses on the free surface vary under different physical parameters. Figures 5a and 6a show the influence of the Weissenberg number, which represents the ratio of elastic to viscous effects in a viscoelastic fluid. As the Weissenberg number increases, elastic forces become more dominant, especially near the corner region where the flow undergoes sharp deformation. In this zone, the fluid's elastic property enables it to store more stress, and the concentrated deformation leads to an increase in both normal and tangential stresses. Figures 5b and 6b highlight the effect of plate speed on stress distribution. A higher plate velocity intensifies the velocity gradient in the fluid, which in turn amplifies the deformation rate. This increase in strain rate raises both normal and tangential stresses due to enhanced stretching and shearing of the fluid near the free surface. Figure 6c demonstrates the effect of the Reynolds number on tangential stress. As the Reynolds number increases, inertial forces begin to outweigh viscous forces. This dominance of inertia elevates the shear rate near the corner, resulting in a rise in tangential stress. However, the stress may act in the reverse direction due to flow reversal or secondary flow structures that develop under strong inertial effects. Overall, these results indicate that geometric singularities such as corners magnify the influence of elasticity, velocity gradients, and inertia on surface stresses. Numerical values of the tangential and normal stresses acting on both the free surface and the plate are computed for various interface angles as shown in Table 3.

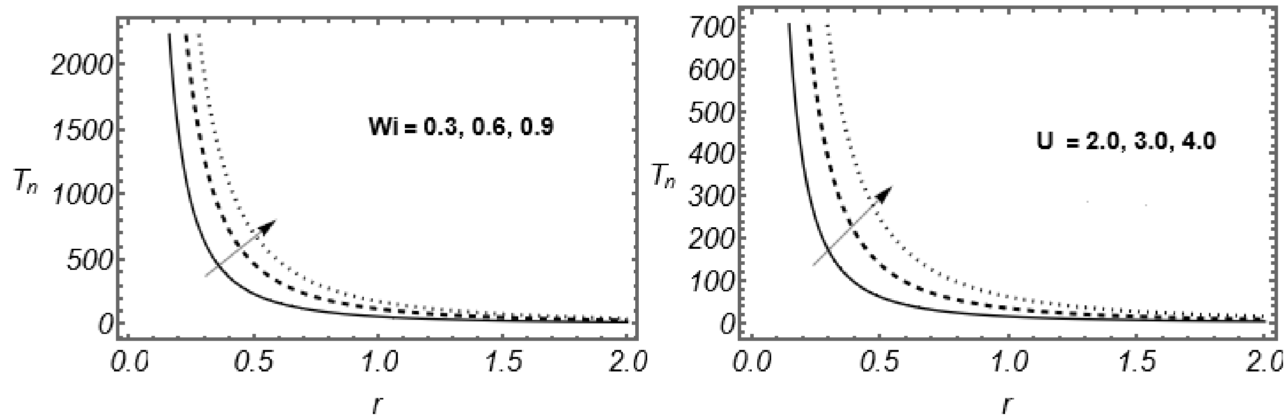

(a) (b)

Figure 5: Variation in normal stress T_n for Wi and U.

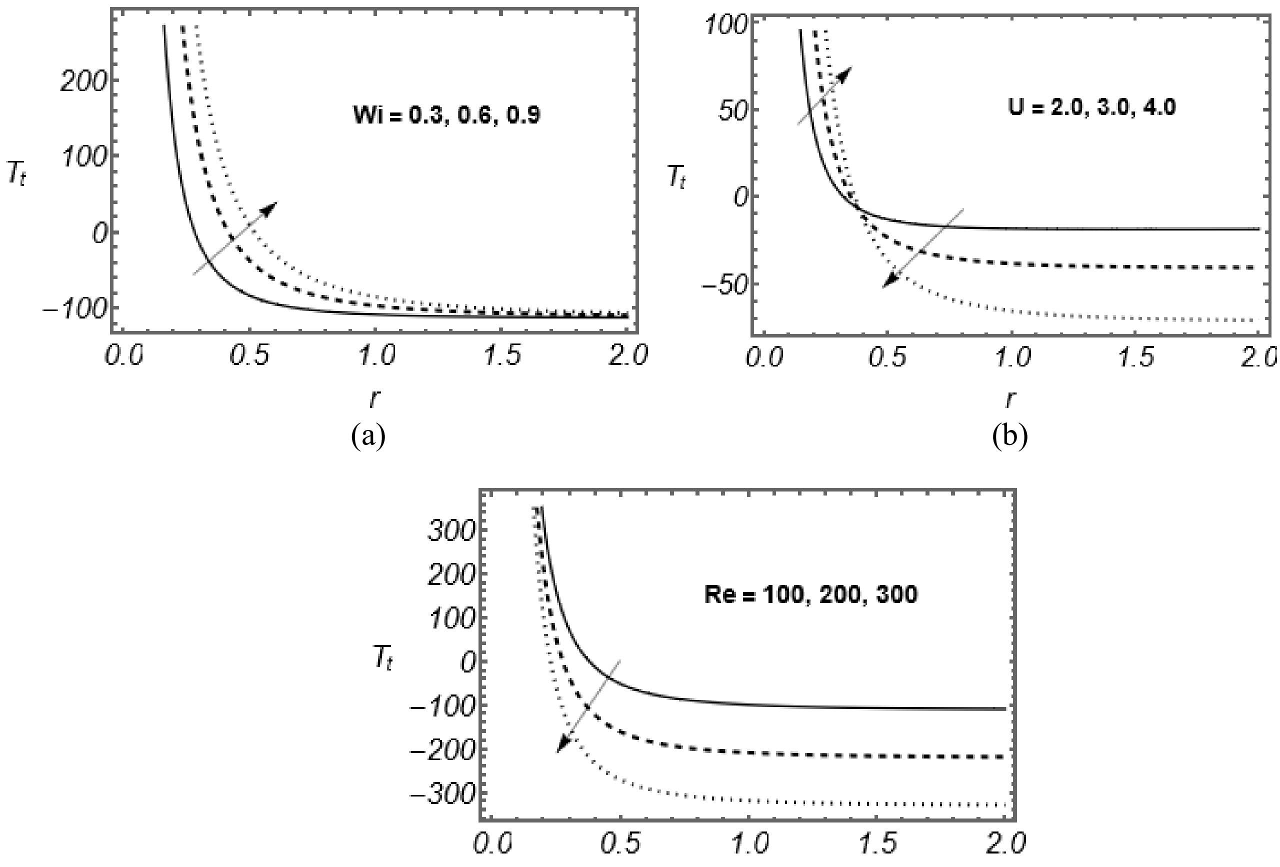

(a) (b)

(c)

Figure 6: Variation in tangential stress T_t for Wi, U and Re.

5.3. Pressure distribution

Corners in a fluid–structure system often act as transition zones where velocity gradients, stresses, and flow direction changes combine to produce noticeable pressure fluctuations. Parameters such as plate length, Weissenberg number, and plate speed directly influence these gradients and stresses, thereby altering the pressure pattern near the corner. Figure 7a shows that when plate length increases, the contact area between the plate and the fluid also increases. Because a larger surface area distributes the applied force over more fluid, the pressure (force per unit area) decreases for the same total applied force. Although corners experience high local stresses, if the overall average pressure is lower due to increased plate length, the corner pressure peak is reduced. Figure 7b illustrates that the Weissenberg number Wi measures the ratio of elastic to viscous effects in a viscoelastic fluid. A higher Wi indicates stronger elastic (memory) effects. When elastic effects dominate, fluid elements resist further compression. Near a corner, where flow direction changes sharply, the fluid is compressed more strongly, resulting in higher local pressure. Figure 7c demonstrates that higher plate speed increases pressure near the corner. This occurs because higher speed amplifies velocity gradients, leading to stronger viscous and elastic contributions. The elevated stress translates into higher pressure peaks, especially at corners where stress concentration is already high.

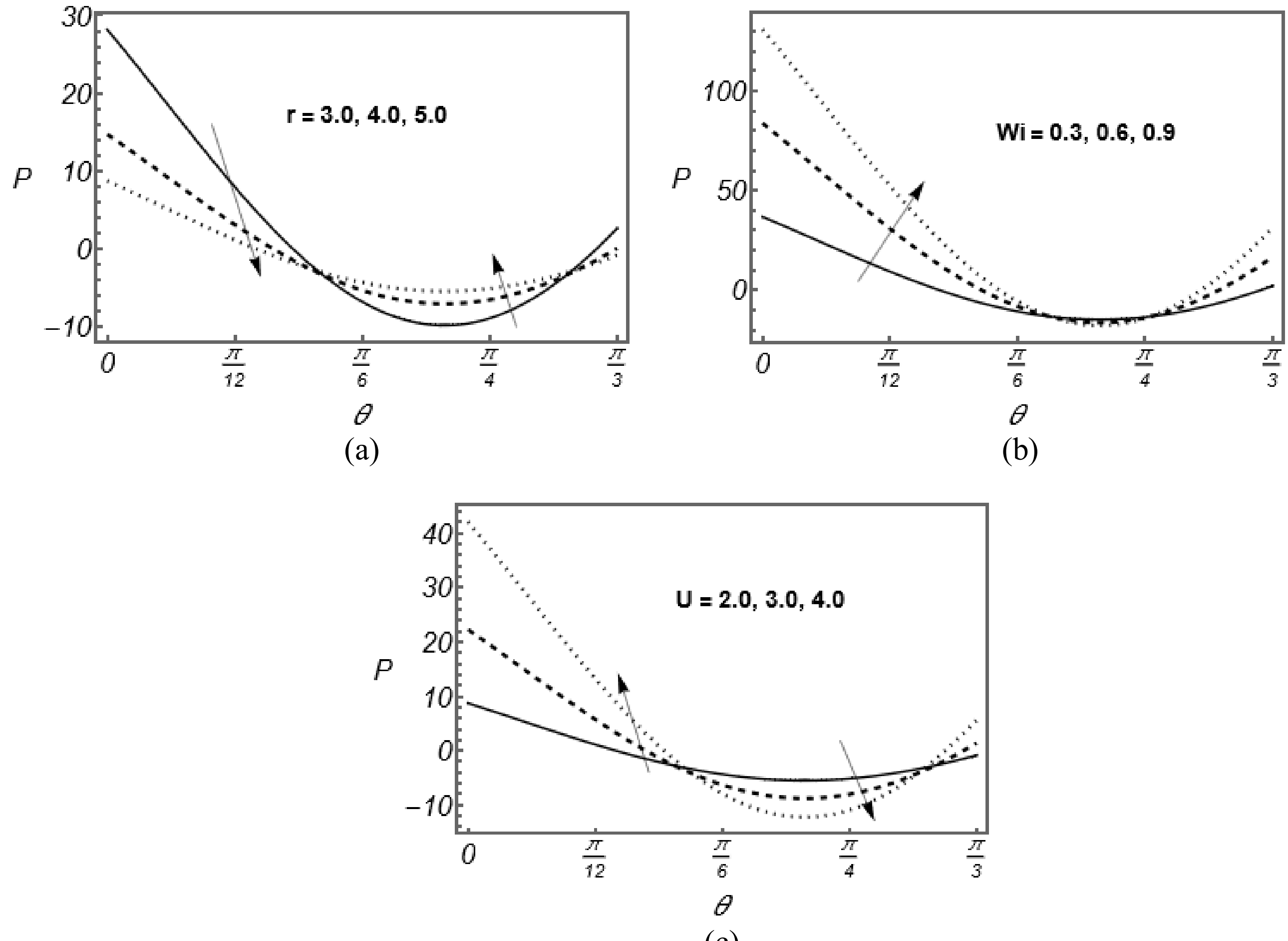

Figure 7: Variation in pressure for r, Wi and U.

5.4. Stream lines

Figure 9 shows how the geometry of the interface specifically the corner angle directly governs fluid motion in the region. When the interface angle is small, the corner acts like a narrow throat, restricting the path available for the fluid. This restriction forces streamlines to crowd together, creating strong velocity gradients, especially near the corner where the fluid is compelled to change direction sharply. As the corner angle increases, the available cross-section for flow becomes larger, reducing confinement. In this wider space, streamlines can spread out more evenly and avoid excessive crowding, which lowers local shear rates and pressure variations. The result is a smoother, more uniform distribution of streamlines because the fluid has more freedom to follow gentle curvatures instead of abrupt turns. In essence, a larger interface angle alleviates geometric constriction, allowing the flow to distribute more evenly and reducing localized disturbances that would otherwise arise from sharp corners.

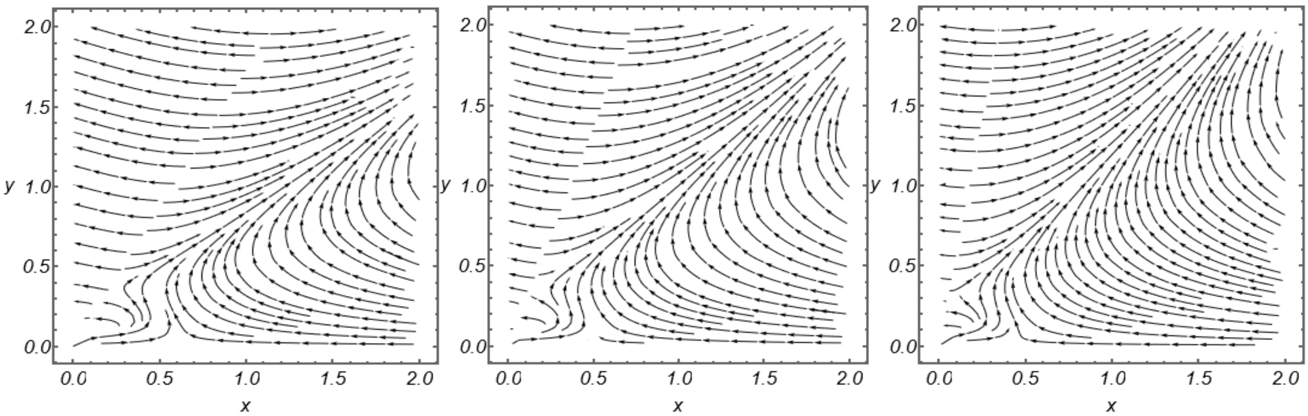

$\theta_0 = 60^0$ (a) $\theta_0 = 70^0$ (b) $\theta_0 = 80^0$ (c)

Figure 8: Streamlines for different variations of θ_0.

Table 1: Error calculated from r-component of momentum equation.

$E_1(r,\theta)$					
r / θ	1.0	1.5	2.0	2.5	3.0
0	-6.984×10^{-6}	-6.984×10^{-6}	-6.984×10^{-6}	-6.984×10^{-6}	-6.984×10^{-6}
15	-8.382×10^{-7}	-2.610×10^{-6}	-2.908×10^{-6}	-2.990×10^{-6}	-3.019×10^{-6}
30	-2.602×10^{-5}	-2.569×10^{-5}	-2.563×10^{-5}	-2.562×10^{-5}	-2.561×10^{-5}
45	-3.248×10^{-6}	-6.416×10^{-7}	-2.030×10^{-7}	-8.315×10^{-8}	-4.010×10^{-8}
60	1.612×10^{-5}	1.813×10^{-5}	1.846×10^{-5}	1.856×10^{-5}	1.859×10^{-5}
90	-3.376×10^{-5}	-3.376×10^{-5}	-3.376×10^{-5}	-3.376×10^{-5}	-3.376×10^{-5}
105	-2.137×10^{-5}	-2.161×10^{-5}	-2.165×10^{-5}	-2.166×10^{-5}	-2.166×10^{-5}

120	4.531×10^{-5}	4.631×10^{-5}	4.648×10^{-5}	4.653×10^{-5}	4.655×10^{-5}
135	-2.698×10^{-5}	-2.775×10^{-5}	-2.788×10^{-5}	-2.791×10^{-5}	-2.792×10^{-5}
150	2.297×10^{-5}	1.890×10^{-5}	1.822×10^{-5}	1.803×10^{-5}	1.797×10^{-5}
165	-8.381×10^{-7}	-2.610×10^{-6}	-2.908×10^{-6}	-2.990×10^{-6}	-3.019×10^{-6}
180	-4.370×10^{-5}	-4.600×10^{-5}	-4.638×10^{-5}	-4.649×10^{-5}	-4.653×10^{-5}

Table 2: Error calculated from θ-component of momentum equation.

$E_2(r,\theta)$					
θ \ r	1.0	1.5	2.0	2.5	3.0
0	7.708×10^{-6}	1.907×10^{-6}	8.147×10^{-7}	0.0	1.591×10^{-7}
15	1.525×10^{-5}	1.525×10^{-5}	4.577×10^{-5}	6.103×10^{-5}	3.051×10^{-5}
30	1.608×10^{-6}	0.0	1.750×10^{-5}	0.0	-1.150×10^{-5}
45	4.924×10^{-6}	0.0	1.653×10^{-5}	0.0	-2.823×10^{-5}
60	1.760×10^{-6}	3.051×10^{-5}	-5.222×10^{-7}	0.0	9.512×10^{-6}
90	-1.395×10^{-5}	0.0	5.675×10^{-5}	0.0	1.131×10^{-5}
105	0.0	0.0	0.0	-1.220×10^{-4}	0.0
120	7.290×10^{-5}	0.0	1.090×10^{-4}	-1.220×10^{-4}	1.012×10^{-4}
135	1.243×10^{-4}	2.441×10^{-4}	2.447×10^{-4}	2.441×10^{-4}	4.062×10^{-4}
150	1.220×10^{-4}	2.441×10^{-4}	4.882×10^{-4}	4.882×10^{-4}	2.441×10^{-4}
165	-1.220×10^{-4}	-4.882×10^{-4}	-2.441×10^{-4}	-4.882×10^{-4}	-9.765×10^{-4}
180	6.370×10^{-5}	0.0	1.155×10^{-4}	0.0	1.769×10^{-4}

Table 3: The numerical values of normal and tangential stress on the free surface and plate at different angle θ_0.

θ_0	$T_t = S_{r\theta}\vert_{\theta=\theta_0}$	$T_n = S_{\theta\theta}\vert_{\theta=\theta_0}$	$L = T_n cos\theta_0 + T_t sin\theta_0$	$D = T_n Sin\theta_0 - T_t Cos\theta_0$
0	∞	∞	∞	∞
15	−25.01	369.4	350.4	119.4
30	−51.09	92.84	54.86	90.66
45	−78.90	42.16	−25.98	85.60
60	−109.7	24.40	−82.82	75.99
90	∞	11.61	∞	11.61
105	−240.3	8.824	−234.4	−53.41

120	−312.2	6.920	−273.8	−150.1
135	−420.8	5.517	−301.4	−293.6
150	−621.8	4.394	−315.3	−536.0
165	−1202	3.423	−316.9	−1160
180	∞	2.533	∞	∞

6. Conclusion

This study examines the influence of inertia on fluid flow when a plate is withdrawn from a liquid bath. A recursive method is employed to solve the resulting nonlinear governing equations, and the solutions are analyzed using both graphical and tabulated results. The analysis reveals the presence of a stress singularity at the corner formed by the plate and the free surface. The results show that both the tangential and normal stresses on the free surface and the plate diverge as the interface angle approaches certain critical values. In particular, the stress normal to the surface and plate, as well as the stress perpendicular to the free surface, becomes unbounded at the critical interface angle. Furthermore, in the case of non-creeping (inertial) flow near a corner, the fluid velocity is significantly higher than in the purely viscous (non-inertial) case. This increase arises from the contribution of inertia, which enhances momentum transport and results in greater fluid motion. In contrast, when inertia is neglected, the velocity field is weaker because these momentum-carrying effects are absent.

Appendix

$$\left(1+\lambda\frac{D}{Dt}\right)\left(\varepsilon \boldsymbol{S}^{(1)}+\varepsilon^2\boldsymbol{S}^{(2)}\right)=\mu\left(\varepsilon {\boldsymbol{A}_1}^{(1)}+\varepsilon^2{\boldsymbol{A}_1}^{(2)}\right),$$

$$\frac{D}{Dt}\left(\varepsilon \boldsymbol{S}^{(1)}+\varepsilon^2\boldsymbol{S}^{(2)}\right)=\left(\left(\varepsilon \boldsymbol{V}^{(1)}+\varepsilon^2\boldsymbol{V}^{(2)}\right).\nabla\right)\left(\varepsilon \boldsymbol{S}^{(1)}+\varepsilon^2\boldsymbol{S}^{(2)}\right)-\left(\varepsilon\nabla \boldsymbol{V}^{(1)}+\varepsilon^2\nabla \boldsymbol{V}^{(2)}\right)\left(\varepsilon \boldsymbol{S}^{(1)}+\varepsilon^2\boldsymbol{S}^{(2)}\right)$$
$$-\left(\varepsilon \boldsymbol{S}^{(1)}+\varepsilon^2\boldsymbol{S}^{(2)}\right)\left(\varepsilon\nabla \boldsymbol{V}^{(1)}+\varepsilon^2\nabla \boldsymbol{V}^{(2)}\right)^T,$$

Continuity equation

$$\varepsilon\left(\frac{1}{r}\frac{\partial\left(ru^{(1)}\right)}{\partial r}+\frac{1}{r}\frac{\partial v^{(1)}}{\partial\theta}\right)+\varepsilon^2\left(\frac{1}{r}\frac{\partial\left(ru^{(2)}\right)}{\partial r}+\frac{1}{r}\frac{\partial v^{(2)}}{\partial\theta}\right)=0,$$

r-component of momentum equation

$$\rho\varepsilon^2\left(u^{(1)}\frac{\partial u^{(1)}}{\partial r}+\frac{v^{(1)}}{r}\frac{\partial u^{(1)}}{\partial\theta}-\frac{{v^{(1)}}^2}{r}\right)=-\frac{\partial\left(\varepsilon p^{(1)}+\varepsilon^2p^{(2)}\right)}{\partial r}+\varepsilon\left(\frac{1}{r}\frac{\partial}{\partial r}\left(rS_{rr}^{(1)}\right)+\frac{1}{r}\frac{\partial S_{r\theta}^{(1)}}{\partial\theta}-\frac{S_{\theta\theta}^{(1)}}{r}\right)$$
$$+\varepsilon^2\left(\frac{1}{r}\frac{\partial}{\partial r}\left(rS_{rr}^{(2)}\right)+\frac{1}{r}\frac{\partial S_{r\theta}^{(2)}}{\partial\theta}-\frac{S_{\theta\theta}^{(2)}}{r}\right),$$

θ-component of momentum equation

$$\rho\varepsilon^2\left(u^{(1)}\frac{\partial v^{(1)}}{\partial r}+\frac{v^{(1)}}{r}\frac{\partial v^{(1)}}{\partial \theta}+\frac{u^{(1)}v^{(1)}}{r}\right)=-\frac{1}{r}\frac{\partial\left(\varepsilon p^{(1)}+\varepsilon^2 p^{(2)}\right)}{\partial \theta}+\varepsilon\left(\frac{1}{r^2}\frac{\partial\left(r^2 S_{r\theta}^{(1)}\right)}{\partial r}+\frac{1}{r}\frac{\partial S_{\theta\theta}^{(1)}}{\partial \theta}\right)+\varepsilon^2\left(\frac{1}{r^2}\frac{\partial\left(r^2 S_{r\theta}^{(2)}\right)}{\partial r}+\frac{1}{r}\frac{\partial S_{\theta\theta}^{(2)}}{\partial \theta}\right)$$

Boundary conditions

$$\left(\left(\varepsilon u^{(1)}+\varepsilon^2 u^{(2)}\right),\left(\varepsilon v^{(1)}+\varepsilon^2 v^{(2)}\right),0\right)=(-\varepsilon U,0,0),\ \ at\ \ \theta=0,$$

$$\left(\left(\varepsilon u^{(1)}+\varepsilon^2 u^{(2)}\right),\left(\varepsilon v^{(1)}+\varepsilon^2 v^{(2)}\right),0\right)=(0,0,0), at\ \ \theta=\theta_0.$$

First-order stress tensor form

$$\left(1+\lambda\frac{D}{Dt}\right)\boldsymbol{S}^{(1)}=\mu\boldsymbol{A_1}^{(1)},$$

$$\frac{D\boldsymbol{S}^{(1)}}{Dt}=0,$$

$$\boldsymbol{A_1}^{(1)}=\left(\nabla\boldsymbol{V}^{(1)}\right)^T+\nabla\boldsymbol{V}^{(1)},$$

$$A_1=0, A_2=\frac{{\theta_0}^2}{sin^2\theta_0-{\theta_0}^2}, A_3=-\frac{sin^2\theta_0}{sin^2\theta_0-{\theta_0}^2}, A_4=\frac{\theta_0-cos\theta_0 sin\theta_0}{sin^2\theta_0-{\theta_0}^2}.$$

$$\begin{aligned}
f_1=\frac{\mathrm{Csc}^2\theta_0}{128k^2(-1+\theta_0\mathrm{Cot}\theta_0)}&(40\theta_0-256\theta_0^3+20\theta+408\theta_0^2\theta-64\theta_0^4\theta\\
&-2(35\theta_0-136\theta_0^3+32\theta_0^5+5\theta+192\theta_0^2\theta-32\theta_0^4\theta)\mathrm{Cos}2\theta_0\\
&-4(-10\theta_0+4\theta_0^3+5\theta+6\theta_0^4\theta)\mathrm{Cos}4\theta_0+(-10\theta_0+10\theta)\mathrm{Cos}6\theta_0\\
&+(-40\theta_0+16\theta_0^3+80\theta+48\theta_0^2\theta+16\theta_0\theta^2)\mathrm{Cos}[4\theta_0-2\theta]\\
&+(10\theta_0-20\theta+8\theta_0\theta^2)\mathrm{Cos}[6\theta_0-2\theta]\\
&+(60\theta_0-152\theta_0^3+32\theta_0^5\mathrm{Cos}-120\theta+96\theta_0^2\theta+64\theta_0^4\theta-96\theta_0\theta^2\\
&-32\theta_0^3\theta^2)\mathrm{Cos}[2(\theta_0-\theta)]+(-40\theta_0+256\theta_0^3+80\theta-336\theta_0^2\theta+112\theta_0\theta^2)\mathrm{Cos}2\theta\\
&+(10\theta_0-120\theta_0^3+32\theta_0^5-20\theta+192\theta_0^2\theta-64\theta_0^4\theta-40\theta_0\theta^2\mathrm{Cos}[2(\theta_0+\theta)]\\
&+32\theta_0^3\theta^2)\mathrm{Cos}[2(\theta_0+\theta)]+(25+24\theta_0^2+192\theta_0^4-240\theta_0\theta-160\theta_0^3\theta)\mathrm{Sin}2\theta_0\\
&+(-20-12\theta_0^2+120\theta_0\theta)\mathrm{Sin}4\theta_0+5\mathrm{Sin}6\theta_0\\
&+(25+12\theta_0^2-40\theta_0\theta-32\theta_0^3\theta+32\theta^2+32\theta_0^2\theta^2)\mathrm{Sin}[4\theta_0-2\theta]\\
&+(-5-20\theta_0\theta-8\theta^2)\mathrm{Sin}[6\theta_0-2\theta]\\
&+(-50-36\theta_0^2-80\theta_0^4+240\theta_0\theta+48\theta_0^3\theta-48\theta^2)\mathrm{Sin}[2(\theta_0-\theta)]\\
&+(-50-36\theta_0^2+32\theta_0^4+280\theta_0\theta-160\theta_0^3\theta-32\theta^2+96\theta_0^2\theta^2)\mathrm{Sin}2\theta\\
&+(25+12\theta_0^2-112\theta_0^4-100\theta_0\theta+176\theta_0^3\theta+8\theta^2-64\theta_0^2\theta^2)\mathrm{Sin}[2(\theta_0+\theta)]\\
&-5\mathrm{Sin}[2(2\theta_0+\theta)])
\end{aligned}$$

$$f_2 = -\frac{\mathrm{Csc}^2\theta_0}{512k^2(-1+\theta_0\mathrm{Cot}\theta_0)}(-24\theta_0 + 128\theta_0^3 - 12\theta - 168\theta_0^2\theta - 64\theta_0^4\theta$$
$$+ 2(21\theta_0 - 56\theta_0^3 - 32\theta_0^5 + 3\theta + 64\theta_0^2\theta + 32\theta_0^4\theta)\mathrm{Cos}2\theta_0$$
$$- 4(6\theta_0 + 4\theta_0^3 - 3\theta - 10\theta_0^2\theta)\mathrm{Cos}4\theta_0 + 6(\theta_0 - \theta)\mathrm{Cos}6\theta_0$$
$$+ 8(3\theta_0 + 2\theta_0^3 - 6\theta - 10\theta_0^2\theta + 2\theta_0\theta^2)\mathrm{Cos}[4\theta_0 - 2\theta]$$
$$+ 2(-3\theta_0 + 6\theta + 4\theta_0\theta^2)\mathrm{Cos}[6\theta_0 - 2\theta]$$
$$+ 4(-9\theta_0 + 10\theta_0^3 + 8\theta_0^5 + 18\theta + 24\theta_0^2\theta + 16\theta_0^4\theta - 24\theta_0\theta^2 - 8\theta_0^3\theta^2)\mathrm{Cos}[2(\theta_0 - \theta)]$$
$$+ 8(3\theta_0 - 16\theta_0^3 - 6\theta + 6\theta_0^2\theta + 14\theta_0\theta^2)\mathrm{Cos}2\theta$$
$$+ 2(-3\theta_0 + 36\theta_0^3 + 16\theta_0^5 + 6\theta - 32\theta_0^2\theta - 32\theta_0^4\theta - 20\theta_0\theta^2 + 16\theta_0^3\theta^2)\mathrm{Cos}[2(\theta_0 + \theta)]$$
$$+ (-15 - 40\theta_0^2 - 64\theta_0^4 + 144\theta_0\theta + 96\theta_0^3\theta)\mathrm{Sin}2\theta_0 + (12 + 20\theta_0^2 - 72\theta_0\theta)\mathrm{Sin}4\theta_0$$
$$- 3\mathrm{Sin}6\theta_0 + (-15 - 20\theta_0^2 + 24\theta_0\theta - 32\theta_0^3\theta + 32\theta^2 + 32\theta_0^2\theta^2)\mathrm{Sin}[4\theta_0 - 2\theta]$$
$$+ (3 + 12\theta_0\theta - 8\theta^2)\mathrm{Sin}[6\theta_0 - 2\theta]$$
$$+ (30 + 60\theta_0^2 + 48\theta_0^4 - 144\theta_0\theta - 80\theta_0^3\theta] - 48\theta^2)\mathrm{Sin}[2(\theta_0 - \theta)]$$
$$+ (30 + 60\theta_0^2 + 32\theta_0^4 - 168\theta_0\theta - 160\theta_0^3\theta - 32\theta^2 + 96\theta_0^2\theta^2)\mathrm{Sin}2\theta$$
$$+ (-15 - 20\theta_0^2 + 16\theta_0^4 + 60\theta_0\theta + 48\theta_0^3\theta + 8\theta^2 - 64\theta_0^2\theta^2)\mathrm{Sin}[2(\theta_0 + \theta)]$$
$$+ 3\mathrm{Sin}[2(2\theta_0 + \theta)])$$

$$k = -1 + 2\theta_0^2 + \mathrm{Cos}2\theta_0$$

$$a_1 = -156\theta_0 - 24\theta_0^3 + 64\theta_0^5 - 16\theta_0(-13 + \theta_0^2)\mathrm{Cos}2\theta_0 + 4(-13\theta_0 + 10\theta_0^3)\mathrm{Cos}4\theta_0$$
$$+ (15 + 152\theta_0^2 - 32\theta_0^4)\mathrm{Sin}2\theta_0 + 4(-3 - 19\theta_0^2)\mathrm{Sin}4\theta_0 + 3\mathrm{Sin}6\theta_0$$

$$a_2 = -132\theta_0 + 88\theta_0^3 - 64\theta_0^5 - 16\theta_0(-11 + 7\theta_0^2)\mathrm{Cos}2\theta_0 + 4\theta_0(-11 + 6)\mathrm{Cos}4\theta_0$$
$$+ (25 + 40\theta_0^2 + 32\theta_0^4)\mathrm{Sin}2\theta_0 - 20(1 + \theta_0^2)\mathrm{Sin}4\theta_0 + 5\mathrm{Sin}6\theta_0$$

$$a_3 = (-3\mathrm{Cos}3\theta_0 + 4\theta_0^2)\mathrm{Cos}3\theta_0 + \mathrm{Cos}5\theta_0 - 2(-1 + 2\theta_0^2)\mathrm{Cos}\theta_0$$

$$a_4 = 2(-5 + 5\theta_0^2 + 2\theta_0^4)\mathrm{Sin}\theta_0 + (5 - 5\theta_0^2 + 4\theta_0^4)\mathrm{Sin}3\theta_0 + (-1 + \theta_0^2)\mathrm{Sin}5\theta_0$$

$$b_1(\theta) = \left(2f_1'^2 + ff_1''\right), b_2(\theta) = (2gf_2 - ff_2''),$$

$$b_3(\theta) = (-2f'(fg)' - 2f'f_1'' - f(fg)'' - ff_1''' + gf_1')$$

$$b_4(\theta) = (-2gf_2' + 2g'f_2 - ff_2'''), b_5(\theta) = \left(-2g(fg)' - 4gf_1'' - 4f'(g^2 + f_1') - 2f(2gg' + f_1'')\right)$$

$$b_6(\theta) = (-4gf_2 + ff_2''), d_1(\theta) = f'f_1' + ff_1'' - b_4' + b_6, d_2(\theta) = -f'f_2' + ff_2'' + 2ff'' + 4ff_2,$$

$$d_3(\theta) = 4b_1 - b_3' + b_5, d_4(\theta) = -ff_2' + 2f'f_2, d_5(\theta) = ff_1' - b_6' - b_4, d_6(\theta) = b_3 - b_5',$$

$$d_7(\theta) = \int (d_4 - 9g_2)d\theta, d_8(\theta) = \int (d_5 + g_1)d\theta, d_9(\theta) = \int (d_6 + 3g_3)d\theta,$$

References

[1] D. R. Ceratti, B. Louis, X. Paquez, M. Faustini, D. Grosso, A New Dip Coating Method to Obtain Large-Surface Coatings with a Minimum of Solution, *Advanced Materials,* Vol. 27, No. 34, pp. 4958-4962, 2015.

[2] M. Dey, F. Doumenc, B. Guerrier, Numerical simulation of dip-coating in the evaporative regime, *The European Physical Journal E,* Vol. 39, No. 2, pp. 19, 2016/02/25, 2016.

[3] L. Landau, B. Levich, *Dragging of a Liquid by a Moving Plate*, in: P. Pelcé, *Dynamics of Curved Fronts*, Eds., pp. 141-153, San Diego: Academic Press, 1988.

[4] R. B. Bird, R. C. Armstrong, O. Hassager, Dynamics of polymeric liquids. Vol. 1: Fluid mechanics, 1986.

[5] J. N. Goodier, LXVI. Additional note on an analogy between the slow motions of a viscous fluid in two dimensions and systems of plane stress, *The London, Edinburgh, and Dublin Philosophical Magazine and Journal of Science,* Vol. 17, No. 114, pp. 800-803, 1934/04/01, 1934.

[6] K. Moffatt, Viscous and Resistive Eddies Near a Sharp Corner, *Journal of Fluid Mechanics Digital Archive,* Vol. 18, pp. 1-18, 01/01, 1964.

[7] S. Taneda, Visualization of Separating Stokes Flows, *Journal of the Physical Society of Japan,* Vol. 46, No. 6, pp. 1935-1942, 1979/06/15, 1979.

[8] K. Moffatt, B. Duffy, Local Similarity Solutions and their Limitations, *Journal of Fluid Mechanics,* Vol. 96, pp. 299-313, 01/29, 1980.

[9] S. Betelu, J. Diez, L. Thomas, R. Gratton, B. Mariño, Instantaneous viscous flow in a corner bounded by free surfaces, *Physics of Fluids,* Vol. 8, pp. 2269, 09/01, 1996.

[10] C. D. Han, L. H. Drexler, Studies of converging flows of viscoelastic polymeric melts. III. Stress and velocity distributions in the entrance region of a tapered slit die, *Journal of Applied Polymer Science,* Vol. 17, No. 8, pp. 2369-2393, 1973.

[11] M. Renardy, Stress integration for the constitutive law of the upper convected Maxwell fluid near the corners in a driven cavity, *Journal of non-newtonian fluid mechanics,* Vol. 112, No. 1, pp. 77-84, 2003.

[12] A. Siddiqui, A. Ansari, A. Ahmad, N. late, On Taylor's scraping problem and flow of a Sisko fluid, *Mathematical Modelling and Analysis,* Vol. 14, pp. 515-529, 12/31, 2009.

[13] J. E. Sprittles, Y. D. Shikhmurzaev, Viscous flow in domains with corners: Numerical artifacts, their origin and removal, *Computer Methods in Applied Mechanics and Engineering,* Vol. 200, No. 9, pp. 1087-1099, 2011/02/01/, 2011.

[14] S. T. Chaffin, J. M. Rees, Carreau fluid in a wall driven corner flow, *Journal of Non-Newtonian Fluid Mechanics,* Vol. 253, pp. 16-26, 2018/03/01/, 2018.

[15] A. Mahmood, Effect of Inertia on Viscous Fluid in a wall-driven Corner Flow with Leakage, *Appl. Math,* Vol. 13, No. 3, pp. 353-360, 2019.

[16] R. Ellahi, Recent trends in coatings and thin film: Modeling and application, 8, MDPI, 2020, pp. 777.

[17] N. Okechi, S. Asghar, Viscoelastic flow through a wavy curved channel, *Chinese Journal of Physics,* Vol. 74, 09/01, 2021.

[18] M. Turkyilmazoglu, Three dimensional MHD flow and heat transfer over a stretching/shrinking surface in a viscoelastic fluid with various physical effects, *International Journal of Heat and Mass Transfer,* Vol. 78, pp. 150-155, 2014/11/01/, 2014.

[19] M. Bhatti, F. Ishtiaq, R. Ellahi, S. Sait, Novel Aspects of Cilia-Driven Flow of Viscoelastic Fluid through a Non-Darcy Medium under the Influence of an Induced Magnetic Field and Heat Transfer, *Mathematics,* Vol. 11, pp. 2284, 05/14, 2023.

[20] S. Shaheen, K. Maqbool, R. Ellahi, S. Sait, Metachronal propulsion of non-Newtonian viscoelastic mucus in an axisymmetric tube with ciliated walls, *Communications in Theoretical Physics,* Vol. 73, pp. 035006, 03/01, 2021.

[21] F. J. Awan, K. Maqbool, S. M. Sait, R. Ellahi, Buoyancy effect on the unsteady diffusive convective flow of a Carreau fluid passed over a coated disk with energy loss, *Coatings,* Vol. 12, No. 10, pp. 1510, 2022.

[22] A. Majeed, A. Zeeshan, S. Z. Alamri, R. Ellahi, Heat transfer analysis in ferromagnetic viscoelastic fluid flow over a stretching sheet with suction, *Neural Comput. Appl.,* Vol. 30, No. 6, pp. 1947–1955, 2018.

[23] H. Alfadil, A. E. Abouelregal, Ö. Civalek, H. F. Öztop, Effect of the photothermal Moore–Gibson–Thomson model on a rotating viscoelastic continuum body with a cylindrical hole due to the fractional Kelvin-Voigt model, *Indian Journal of Physics,* Vol. 97, No. 3, pp. 829-843, 2023.

[24] A. Zeeshan, H. Javed, N. Shehzad, S. Sait, R. Ellahi, An integrated numerical and analytical investigation on cilia-generated MHD flow of Jeffrey fluid through a porous medium, *International Journal of Numerical Methods for Heat & Fluid Flow,* Vol. 34, 08/30, 2024.

[25] M. M. Bhatti, R. Ellahi, S. Sait, R. Ullah, Exact solitary wave solutions of time fractional nonlinear evolution models: a hybrid analytic approach, *Bulletin of the Transilvania University of Brasov. Series III: Mathematics and Computer Science*, pp. 83-98, 09/03, 2024.

[26] W. Langlois, *A RECURSIVE APPROACH TO THE THEORY OF SLOW, STEADY-STATE VISCOELESTIC FLOW*, pp. 1962.

[27] W. Langlois, The recursive theory of slow viscoelastic flow applied to three basic problems of hydrodynamics, *Journal of Rheology*, 1964.

[28] A. Mahmood, A. Siddiqui, Two dimensional inertial flow of a viscous fluid in a corner, *Applied Mathematical Sciences,* Vol. 11, pp. 407-424, 01/01, 2017.

[29] G. Taylor, On scraping viscous fluid from a plane surface, *The Scientific Papers of Sir Geoffrey Ingram Taylor*, No. 1971, pp. 410-413, 1962.